RSC Advances

PAPER

View Article Online
View Journal | View Issue

Cite this: *RSC Adv.*, 2021, **11**, 18994

Waste eggshell membrane-templated synthesis of functional Cu^{2+}–Cu^{+}/biochar for an ultrasensitive electrochemical enzyme-free glucose sensor†

Linzhi Li,‡[a] Tianzeng Huang,‡[b] Saijun He,[a] Xing Liu,[a] Qi Chen,[a] Jian Chen[ac] and Hongmei Cao*[ac]

A fast and sensitive test of blood glucose levels is very important for monitoring and reducing diabetic complications. Herein, a simple and sensitive non-enzymatic glucose sensing platform was fabricated by employing Cu^{2+}–Cu^{+}/biochar as the catalyst. The Cu^{2+}–Cu^{+}/biochar was synthesized through a bio-inspired synthesis, in which waste eggshell membrane (ESM) was introduced as a template to absorb Cu^{2+}, then converting it into Cu^{2+}–Cu^{+} biochar *via* a rapid pyrolysis. The structure and properties of the as-prepared Cu^{2+}–Cu^{+} biochar were determined by scanning electron microscopy (SEM), FT-IR spectroscopy, Raman spectroscopy and cyclic voltammetry (CV). Due to great advantages of Cu^{2+}–Cu^{+}/biochar, such as high electrical conductivity, unique three-dimensional porous network and large electrochemically active surface area, the as-prepared Cu^{2+}–Cu^{+} biochar modified electrode showed high catalytic activity towards glucose oxidization. The fabricated enzyme-free glucose sensor showed excellent performance for glucose determination with a linear range of 12.5–670 μM, and a limit of detection (LOD) of 1.04 μM. Moreover, the as-fabricated sensor has good anti-interference ability and stability. Finally, the proposed senor has been successfully applied to detect glucose in clinical samples (human serum). Owing to the green synthesis method, using biowaste ESM as a template, and the superior catalytic performance and low cost of Cu^{2+}–Cu^{+}/biochar, the developed sensor shows great potential in clinical applications for direct sensing of glucose.

Received 13th January 2021
Accepted 19th May 2021

DOI: 10.1039/d1ra00303h

rsc.li/rsc-advances

Introduction

Nowadays, diabetes has become a worldwide public health problem. Diabetes as a chronic disease, can cause some serious complications, such as kidney failure, stroke, heart disease, and so on.[1] Therefore, a reliable and accurate determination of blood glucose level is of great significance for the prompt treatment and stringent control of diabetes. To date, electrochemical sensors have been widely applied to monitor the glucose concentration, attributed to their rapid response, simplicity, high sensitivity and selectivity and low cost.[2,3] Glucose enzymatic biosensors based on glucose oxidase (GOx) possess excellent sensitivity and selectivity, playing a key role in simple easy-to-use blood sugar testing.[4,5] However, they still have some drawbacks, such as chemical and thermal instability, complicated immobilization process, high cost of enzyme and so on.[6] Hence, the design and fabrication of high performance and cost-effective non-enzymatic glucose sensors is extremely desirable.

With the great advances of nanotechnology, a class of special nanomaterials *via* bio-inspired synthesis method has aroused the focus of researchers in recent years.[7] The researchers make great effort to use a large number of biological materials including bacteria,[8] butterfly wings,[9] viruses,[10] proteins,[11] and the eggshell membrane (ESM) as templates for nanomaterials synthesis, widely employing for catalysis, energy conversion, water pollution, medicine and sensor.[12–14] Among them, the waste ESM from the economic and abundant agricultural byproduct is a naturally-occurring biomaterial regarded as a biowaste. In fact, the ESM is a hierarchically assembled porous composite, which is composed of 95% $CaCO_3$ minerals and about 3.5% of glycoproteins, proteins and proteoglycan.[15,16] Due to the significant industrial applications of $CaCO_3$, eggshell holds great business potential if it can be integrated with metal ions into functional nanocomposites.[17] Furthermore, the ESM has unique interwoven fiber network, and a large number of functional groups (–COOH, $–NH_2$, –OH) on the surface, which makes it an excellent bio-template for constructing nano-structures. Thus, many researchers devote much efforts to

[a]*College of Food Science and Technology, Hainan University, 58 Renmin Avenue, Haikou 570228, China. E-mail: hmcao@hainanu.edu.cn*

[b]*College of Chemistry and Engineering Technology, Hainan University, 58 Renmin Avenue, Haikou 570228, China*

[c]*Key Laboratory of Food Nutrition and Functional Food of Hainan Province, 58 Renmin Avenue, Haikou 570228, China*

† Electronic supplementary information (ESI) available. See DOI: 10.1039/d1ra00303h

‡ These authors contributed equally to this work.

using the ESM as a biological template for the synthesis of nanocomposites with various applications. For example, He *et al.* took advantages of ESM as template for synthesis CuO–ZnO nanocomposites for enhanced water purification.[18] Huang *et al.* synthesized ESM-derived $CaCO_3$/MgO nano-composites for improving bone regeneration.[19] Ding *et al.* reported conversion of ESM into difunctional Au/$CaCO_3$ nanocomposite, thus generating an efficient catalyst for 4-nitrophenol electrochemical detection.[20] Meanwhile, Ding *et al.* also used AuNP/ESM for surface-enhanced Raman spectroscopy detection of thiabendazole in oolong tea.[21] Markovski *et al.* described the waste ESM modified by goethite/α-MnO_2 for arsenate removal.[22] Zhong *et al.* developed 3D hierarchical porous Au networks for electrochemical nonenzymatic glucose sensor with high sensitivity and selectivity.[23] Compared with various noble metal nanoparticles, such as Au, Pd and Pt, Cu has been paid much attention owing to high catalytic and conductive properties, good stability, especially low cost, which has great potential in various applications. Although Cao *et al.* synthesized Cu^{2+}–Cu^{+}/biochar for electrochemical detection of nitrite in water,[24] until now few studies are reported that it is explored for electrochemical glucose detection. Herein, we prepared highly stable copper ion-containing biochar materials by a green and sustainable method, which was further applied for ultrasensitive enzyme free glucose sensing. ESM with unique three-dimensional structure can provide larger specific surface areas and more adsorption sites for electrochemical reactions. Furthermore, ESM could effectively immobilize and disperse nanoparticles, attributed to a rigid structure of porous network preventing nanoparticle aggregation. These excellent characteristics make Cu^{2+}–Cu^{+}/biochar as an efficient and robust electrocatalytic interface material for catalysing the oxidization glucose without loading any enzymes. Thus, in this work, an enzyme-free electrochemical glucose sensor is fabricated. Furthermore, the developed sensing exhibited high sensitivity, low detection limit, and strong anti-interference property. Finally, the optimized sensing was used to successfully determine the glucose level in human serum. All results indicated that the Cu^{2+}–Cu^{+}/biochar might be as excellent materials for enzyme free electrochemical sensor.

Experimental

Reagents and materials

Potassium ferricyanide and potassium ferrocyanide were purchased from Aladdin Co. Ltd. (Shanghai, China). KCl, NaOH and NaCl were ordered from Xilong Chemical Co. Ltd. (Guangzhou, China). $HAuCl_4 \cdot 3H_2O$, vitamin C (VC) and Nafion were obtained from Sinopharm Chemical Reagent (Shanghai, China). Uric acid (UA), and dopamine (DA) were received from Maclean Biotechnology Co., Ltd. (Shanghai, China). D-(+)-Glucose and human serum were bought from Solarbio Science & Technology Co., Ltd. (Beijing, China). Eggshell membrane (EMS) used in this work was got from the canteen at Hainan University. Deionized water was prepared from the Millipore water purification system (18.2 MΩ cm, Milli-Q) and used to prepare all solutions. All of other reagents were of analytical grade.

Apparatus

All of the cyclic voltammetry (CV), electrochemical impedance spectroscopy (EIS) and chronoamperometry (*i*–*t*) experiments were performed with the CHI660e electrochemistry workstation (Shanghai CH Instruments, China). The conventional three-electrode electrochemical system was used in the study that include a glassy carbon electrode (GCE, diameter 3 mm) as working electrode, the saturated calomel electrode (SCE) as reference electrode, and a Pt-wire as counter electrode. The size and morphologies of the natural eggshell membrane and the calcined Cu^{2+}–Cu^{+}/biochar composite were recorded by field-emission scanning electron microscope (FESEM, Zeiss, Germany, accelerating voltage 15 kV). Fourier transform infrared spectroscopy (FT-IR) measurements were performed by a Thermo Nicolet FTIR spectrometer in the range of 4000 to 700 cm^{-1} under transmission sampling mode. The Raman signals of the sample were obtained with a Raman spectrometer (Renishaw in Via, UK).

Synthesis of functional Cu^{2+}–Cu^{+}/biochar

The Cu^{2+}–Cu^{+}/biochar composites *via* ESM as the template were synthesized according to the literature with light modification.[24] Scheme 1 illustrates the synthesis of functional Cu^{2+}–Cu^{+}/biochar at preparation part. First, fresh eggshells were carefully washed with plenty of water. Then the ESM was carefully peeled from a broken fresh eggshell after removing residual proteins and yolk. The stripped ESM were washed thoroughly with deionized water, and then dried at room temperature, and grinded into powder. Afterwards, 1 g of the ESM powder were immersed into 50 mL of 0.05 M $CuCl_2$ solution and stirred magnetically for 24 h. Next, 20 mL of VC (0.1 M) solution was poured into mentioned solution (copper chloride solution containing ESM) with constant stirring for another 24 h. The sample was filtered, rinsed with large amounts of deionized water to remove excess $CuCl_2$ and then dried at 60 °C in an oven. Finally, the samples were placed in a muffle furnace and calcined at 250 °C in the air atmosphere for 3 h to produce Cu^{2+}–Cu^{+}/biochar. The resulting black powder of Cu^{2+}–Cu^{+}/biochar was collected and stored at 4 °C for further use.

Fabrication of Cu^{2+}–Cu^{+}/biochar modified electrode

Moreover, the fabrication process of the nonenzyme glucose sensing based Cu^{2+}–Cu^{+}/biochar is illustrated in Scheme 1. First, the glassy carbon electrode surface (diameter 3 mm, nominal surface area about 0.071 cm^2) polished with 0.3 μm

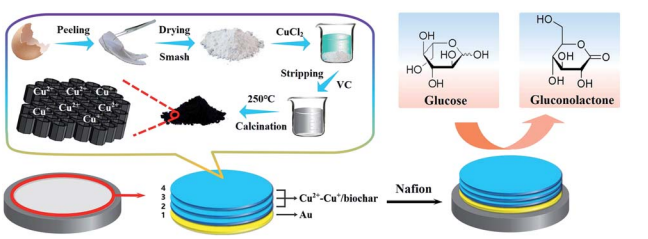

Scheme 1 The fabrication process of the nonenzyme glucose sensing based Cu^{2+}–Cu^{+}/biochar.

and 0.05 μm alumina polishing powder, followed by successive ultrasonic processing with ethanol and deionized water for 2 min respectively, and then the electrode surface was dried with the nitrogen. Then, the prepared working electrode was immersed in 1% $HAuCl_4$ solution and the nano-Au layer was electrodeposited at a potential of −0.2 V for 50 s (SCE as reference electrode). Next, 5 μL of 2 mg mL^{-1} Cu^{2+}–Cu^{+} biochar dispersion was added dropwise to the surface of the electrode and dried at room temperature. Such the operation was repeated for three times. Finally, 5 μL 1% Nafion solution was added to the surface of modified electrode. The obtained modified electrode is stored at 4 °C for further use.

Results and discussion

Structural characterization of Cu^{2+}–Cu^{+}/biochar

To determine the detailed morphology of prepared Cu^{2+}–Cu^{+}/biochar. FESEM was used to demonstrate the structure characters of natural eggshell membrane and calcined Cu^{2+}–Cu^{+}/biochar nanocomposites. From Fig. 1A and C, it is obvious to investigate the alternating 3D network structure of the ESM containing collagen and glycoproteins. Moreover, a natural and porous structure with a large number of functional groups (such as amino and carboxyl groups) of ESM easily adsorb a large amount of metal ions or nanoparticles. The calcined Cu^{2+}–Cu^{+}/biochar loaded with a large amount of Cu^{2+} and Cu^{+} are shown in Fig. 1B and D under different magnifications. As shown in Fig. 1B, there is a large amount of Cu^{2+}–Cu^{+} metal ions coated on the porous three-dimensional structure surface of the materials to improve the conductance. Furthermore, SEM images of after gold deposition and Au/Cu^{2+}–Cu^{+}/biochar modified electrode are shown in Fig. S1.† After gold deposition in GCE, uniform size of gold nanoparticles can be clearly observed on the electrode surface in Fig. S1A,† and Cu^{2+}–Cu^{+}/biochar distributed on the gold nanoparticles can be seen in Fig. S1B.† The elemental composition analysis of Au/Cu^{2+}–Cu^{+}/biochar by EDS technique (Fig. S2 in ESI†) demonstrated that Cu^{2+}–Cu^{+}/biochar mainly is composed of Cu, C, N, and O elements. The ESM will contain high C and N elemental signals after high temperature treatment according to reported literature. Therefore, our result is consistent with the reported literature.[24]

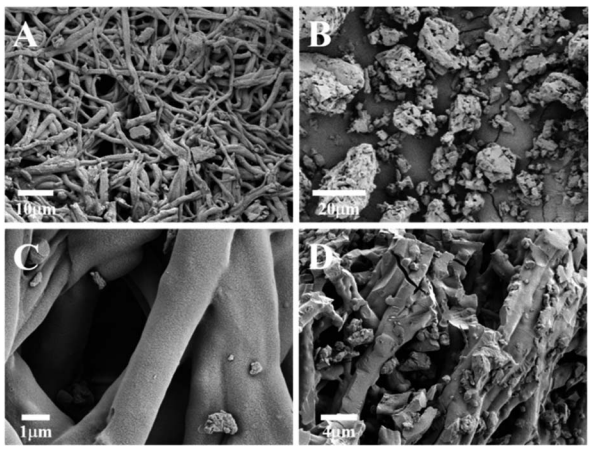

Fig. 1 FESEM images of the natural eggshell membrane (A, C) and the calcined Cu^{2+}–Cu^{+}/biochar composite (B, D).

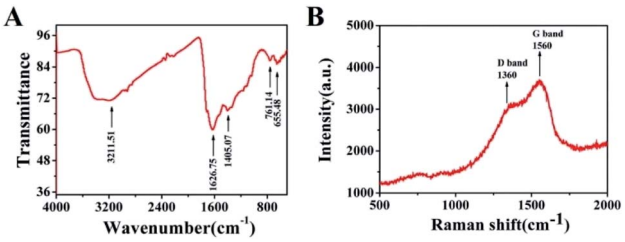

Fig. 2 (A) FT-IR spectra of Cu^{2+}–Cu^{+}/biochar; (B) Raman spectra of Cu^{2+}–Cu^{+}/biochar composite.

Spectral characterization

Furthermore, FT-IR and Raman spectra was used to characterize the molecular structures of the Cu^{2+}–Cu^{+}/biochar composite materials. From characteristic FT-IR spectra of Cu^{2+}–Cu^{+}/biochar (Fig. 2A), it was evident that the broadest peak at 3410 cm^{-1} corresponded to the stretching vibrations of O–H, and the peak at 1405 cm^{-1} corresponded to the stretching vibrations of C–O.[25] The peak at 1626 cm^{-1} could be attributed to the C=O tensile vibration. The result is almost consistent with reported literature. Moreover, Raman spectra was also explored for characterization of Cu^{2+}–Cu^{+}/biochar. As shown from Fig. 2B, there is a significant D-band (1360 cm^{-1}) and G-band (1560 cm^{-1}) in Cu^{2+}–Cu^{+}/biochar. These two peaks could demonstrate the existence of C–H and C=C, respectively,

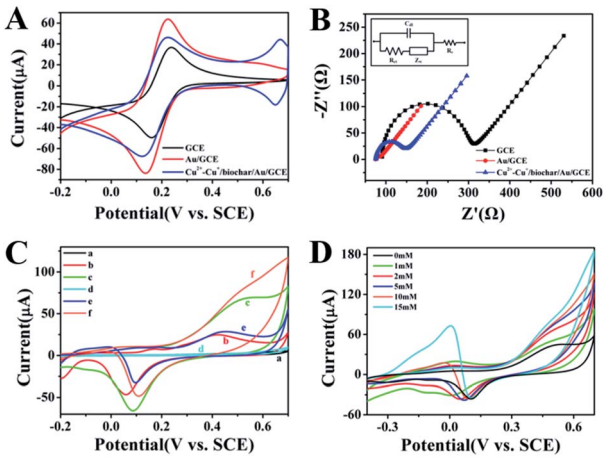

Fig. 3 (A) CV curves of bare GCE, Au/GCE and Cu^{2+}–Cu^{+}/biochar/Au/GCE in 5 mM $[Fe(CN)_6]^{3-}$ and 0.1 M KCl solution with the scan rate of 0.1 V s^{-1}; (B) Nyquist plots of EIS of bare GCE, Au/GCE and Cu^{2+}–Cu^{+}/biochar/Au/GCE in 10 mM $[Fe(CN)_6]^{3-/4-}$ (1 : 1) and 0.1 M KCl solution in the frequency range of 10^{-1} to 10^{5} Hz (inset: the fitting equivalent circuit); (C) CV curves of bare GCE (a, d), Au/GCE (b, e) and Cu^{2+}–Cu^{+}/biochar/Au/GCE (c, f) in 0.1 M NaOH electrolyte solution with and without 5 mM glucose; (D) CV curves of Cu^{2+}–Cu^{+}/biochar/Au/GCE towards various glucose concentrations in 0.1 M NaOH electrolyte solution.

which was similar to the Raman spectra of graphene,[26] indicating that the graphitized structure of the ESM adsorbed by Cu^{2+} was maintained after carbonization. The D and G bands nearly merged into one peak attributed to doped metal nanoparticles.

Electrochemical characterization of the sensor

As presented in Fig. 3A, the cyclic voltammogram (CV) curves of bare GCE, Au/GCE and Cu^{2+}–Cu^{+}/biochar/Au/GCE in KCl solution containing 5 mM $[Fe(CN)_6]^{3-/4-}$ were investigated. The CV curve of bare GCE displayed a reversible pair of anodic and cathodic peaks. After electrodeposition of Au layer, the CV peak current increased compared to GCE due to Au nanoparticles with high conductivity. After modification of Cu^{2+}–Cu^{+}/biochar, the CV peak current of Cu^{2+}–Cu^{+}/biochar/Au/GCE slightly decreases compared with Au/GCE, but larger than that of GCE, indicating Cu^{2+}–Cu^{+}/biochar increasing electron transfer to some extent. Electrochemical impedance spectroscopy (EIS) is generally applied to characterize the assembly of modified electrodes due to providing sensitive and immediate responses to changes in electroactive substances. Fig. 3B, Nyquist plots of the different modified electrodes were obtained using $[Fe(CN)_6]^{3-/4-}$ as the electroactive redox probe. After the electrodeposition of Au, the Nyquist plots displayed an almost straight line, with the R_{et} value of 15 Ω (curve b, inset), which is lower than that of the GCE (240 Ω). The results reflect acceleration in electron transfer between redox probe and Au surface due to the high conductivity properties of AuNPs. When the assembly of Cu^{2+}–Cu^{+}/biochar, R_{et} slightly increased at approximately 70 Ω because the Cu^{2+}–Cu^{+}/biochar partly impeded the electron transfer of $[Fe(CN)_6]^{3-/4-}$ compared with electrodeposition Au layer. However, its R_{et} value is lower than that of the GCE, suggesting acceptable conductivity of Cu^{2+}–Cu^{+}/biochar. Moreover, we observed pH effect on the oxidation state of the Cu and the functional groups on the biochar surface in CV and EIS test (Fig. S4†). We obtained similar characterization curves in NaOH solution in Fig. S4,† indicating that pH has little effect on the oxidation state of the Cu and the functional groups on the biochar surface in EIS and CV tests. In addition, we investigated CV of the GCE, Au/GCE, Cu^{2+}–Cu^{+}/biochar/Au/GCE in 0.1 M NaOH with and without glucose. As shown in Fig. 3C, the gold nanoparticles showed an oxidation peak at 0.6 V, and the oxidation current increased with the presence of glucose in the NaOH solution. After the electrode modified with the Cu^{2+}–Cu^{+}/biochar, the oxidation current increased further. This means that both AuNPs and Cu^{2+}–Cu^{+}/biochar have a synergy catalytic effect on glucose. Moreover, we also investigate catalytic performance of Cu^{2+}–Cu^{+}/biochar/Au/GCE in glucose oxidation. As shown in Fig. 3D, when the glucose concentration continuously increased from 0 mM to 15 mM, the oxidation current increased, implying that the prepared sensor had a good catalytic effect on glucose oxidation. Between 0 V and 0.6 V, oxidation peak current was related to the transition of Cu(I) to Cu(II) and Cu(II) to Cu(III). At the potential of 0.6 V, oxidation peak current is attributed to Cu(II)–Cu(III) conversion, and at potential near 0 V refers to the oxidation of Cu(I) to Cu(II). Moreover, the glucose is direct electrochemical oxidized to gluconolactone. Meanwhile, we also observed the reduction peak of AuNPs at the potential of 0.1 V in Fig. 3D. When the concentration of glucose gradually increased, new reduction peak of glucose appeared at the potential of −0.1 V, attributed to further oxidation gluconolactone by AuNPs. It is well known that the oxidization of glucose greatly depended on the amount of Au and Cu^{2+}–Cu^{+}/biochar. Thus, the electrocatalytic activity towards glucose on sensor may result from the synergistic catalytic effect AuNPs and Cu^{2+}–Cu^{+}/biochar. In addition, we observed the effects of different scan rates on the oxidation of glucose at the Cu^{2+}–Cu^{+}/biochar/Au/GCE. The CV of the Cu^{2+}–Cu^{+}/biochar/Au/GCE electrode was presented in Fig. S3† for glucose oxidation at different scan rates (30–500 mV s^{-1}) in 0.1 M NaOH solution. As shown in Fig. S3,† the electric current density is proportional to the square root of the scan rate, suggesting that the electrocatalytic reaction is diffusion-controlled process.

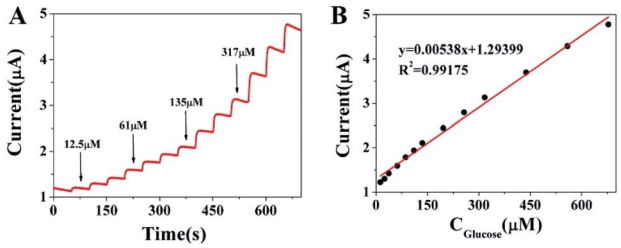

Fig. 4 (A) Amperometric response of Cu^{2+}–Cu^{+}/biochar/Au/GCE to the successive addition of glucose and (B) the corresponding calibration curve.

Amperometric response of the sensor towards glucose

Fig. 4 illustrates the amperometric responses of the Cu^{2+}–Cu^{+}/biochar/Au/GCE for successive addition of various concentrations of glucose at a working potential of 0.6 V and the sample interval of 0.1 s (*vs.* SCE) in 0.1 M NaOH solution. For achieving a homogeneous glucose concentration instantly, the solution was vigorously stirred to ensure well-distributed of glucose and electrolyte. As shown in Fig. 4A, upon addition of the glucose solution, the Cu^{2+}–Cu^{+}/biochar/Au/GCE reaches a dynamic equilibrium within 3 s, suggesting a very fast amperometric response of modified electrode. Fig. 4B shows the calibration curve of glucose at the Cu^{2+}–Cu^{+}/biochar/Au/GCE. The proposed electrode displays a linear response to glucose in the range from 12.5 μM to 670 μM and a low detection limit of 1.04 μM at a signal/noise ratio of 3. The corresponding regression equation is $I\,(\mu A) = 0.00538C\,(\mu M) + 1.29399$ ($R^2 = 0.99175$). For comparison, the performances of our sensor and other glucose sensors reported in literatures have been listed in Table 1. From Table 1, it can be concluded that the developed sensor has a lower detection limit, higher sensitivity and a quite wider linear range than those reported previously. The higher sensitivity was attributed to the fact that on the one hand, Cu^{2+}–Cu^{+}/biochar can greatly increase

Table 1 Comparison of the performances of our sensor and other glucose sensors reported literatures

Type of the electrode	Linear range (mM)	Detection limit (μM)	Ref.
Cu–CuO/PANI/316L	0.1–5	100	27
GOD/SBP_{Thi}/GCE	8.2×10^{-4} to 4.0	0.27	28
Poly-AAM/Au-SPE/MIP	0.5–50 μg mL^{-1}	0.59	29
Ni–Co–S/PPy/NF	2×10^{-3} to 2	0.82	30
S–Cu_2O/Nafion/GCE	0.05–5.65	1.7	31
C–Cu_2O/Nafion/GCE	0.05–7.15	1.13	31
SWCNTs/Cu_2O/ZnO NRs/graphene hybrid electrodes	0.6–11.1	—	32
MWCNTs-BCS/Cu/GOx/Naf	0.01–0.49	2	33
CuS-W/E/GC	0.02–2.5	2	34
PC platinum/Cu_2O	0.1–2.5	26	35
NF/octahedral Cu_2O/GCE	0.1–5.0	5.11	36
Cu^{2+}–Cu^{+}/Au/GCE	0.0125–0.67	1.04	This work

the electrocatalytic active areas, on the other hand, synergistic effect between Au nanoparticles and Cu^{2+}–Cu^{+}/biochar with high electrocatalytic activity.

Specificity, reproducibility and stability of the non-enzyme sensing

To evaluate the specificity of the developed sensors, possible interfering species, dopamine (DA), VC, and uric acid (UA) normally coexisting with glucose in human blood, were examined. Considering that the concentration of glucose is about 30 times of the interfering species in the human blood, thus normal physiological levels of glucose (5 mM), VC (0.025 mM), UA (0.025 mM), 0.1 mM NaCl and DA (0.025 mM) were orderly added into 0.1 M NaOH solution at a potential of 0.6 V by amperometric responses. The results are shown in Fig. 5. The results demonstrate our fabricating sensor has high selectivity and reliable anti-interference property by comparing the amperometric responses with other relevant interfering species. Moreover, the good reproducibility and long-term stability of the sensor are the significant factor of sensor performance. Thus, the storage stability was observed at intervals by measurement toward 0.5 mM glucose in 0.1 M NaOH solution, and the sensor was stored at room temperature when not in use.

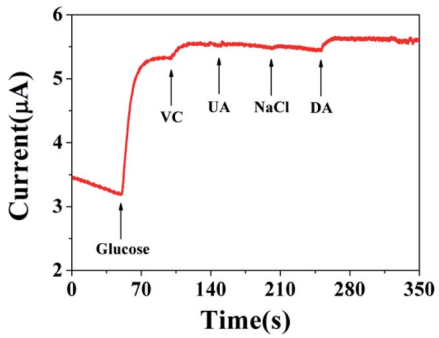

Fig. 5 Amperometric response curve of Cu^{2+}–Cu^{+}/biochar/Au/GCE obtained in the presence of 0.1 M NaOH at +0.6 V with continuous stirring to the successive addition of 5 mM glucose, 0.025 mM VC, 0.025 mM UA, 0.1 mM NaCl and 0.025 mM DA.

The result displayed that it still remained 91.79% of initial catalytic current response after 2 weeks, indicating the satisfactory stability of the as-fabricated nonenzymatic glucose sensor. The intra-assay precision of sensors was estimated by detecting 5 mM glucose at 0.6 V at two electrodes for successive 3 measurements, the relative standard deviation (RSD) was 0.998%, signifying a good intra-assay precision. The reproducibility of the sensor for glucose detection was evaluated using three replicate measurements from the batch; RSD was 0.786%, indicating that the fabrication method was highly reproducible. Therefore, the prepared Cu^{2+}–Cu^{+}/biochar is an excellent candidate for the fabrication of sensitive, stable and specific amperometric sensor for the non-enzymatic detection of glucose.

Application of glucose determination in human serum

In order to further verify the feasibility of the developed sensor for analysis of glucose, Cu^{2+}–Cu^{+}/biochar/Au/GCE was employed to detect the glucose in human serum. The quantitative determination of human serum sample was carried out by the standard addition method and the obtained results were presented in Table 2. The good recovery ratios of the samples indicate that the proposed sensor can be successfully applied in detecting the concentration of glucose in human serum.

Table 2 Results of glucose detection in human serum samples

Sample	Added (μM)	Detected (μM)	Average (μM)	Recovery (%)	RSD (%)
1	50	48.95	49.70	99.38	1.62
		50.55			
		49.59			
2	250	254.83	253.25	101.30	0.78
		253.88			
		251.05			
3	500	518.30	510.78	102.16	1.77
		500.75			
		513.30			

Conclusions

We synthesized Cu^{2+}–Cu^{+}/biochar *via* the waste eggshell membrane (ESM) as template. Furthermore, as-synthesized materials have been used to successfully construct non-enzymatic glucose sensors. The proposed sensor exhibited a rapid response, large linear range, a low detection limit with satisfactory stability, and repeatability, attributed to synergistic effect of AuNPs and Cu^{2+}–Cu^{+}/biochar with large surface. Finally, it can be applied for detection of glucose content in human serum samples. Thus, the fabricated sensor has the potential for providing a noninvasive route of monitoring glucose for diabetic patients.

Conflicts of interest

There are no conflicts to declare.

Acknowledgements

This work was supported by Hainan Provincial Natural Science Foundation of China (320QN204 and 2019RC129) and the Scientific Research Foundation of Hainan University (grant number KYQD(ZR)1939, KYQD(ZR)1952).

References

1 J. Wang, *Chem. Rev.*, 2008, **108**, 814–825.
2 H. Cao, A. Yang, H. Li, L. Wang, S. Li, J. Kong, X. Bao and R. Yang, *Sens. Actuators, B*, 2015, **214**, 169–173.
3 D. Ye, G. Liang, H. Li, J. Luo, S. Zhang, H. Chen and J. Kong, *Talanta*, 2013, **116**, 223–230.
4 C. Hu, D. Yang, F. Zhu, F. Jiang, S. Shen and J. Zhang, *ACS Appl. Mater. Interfaces*, 2014, **6**, 4170–4178.
5 C. You, X. Xu, B. Tian, J. Kong, D. Zhao and B. Liu, *Talanta*, 2009, **78**, 705–710.
6 L. Meng, J. Jin, G. Yang, T. Lu, H. Zhang and C. Cai, *Anal. Chem.*, 2009, **81**, 7271–7280.
7 J. Huang, L. Lin, D. Sun, H. Chen, D. Yang and Q. Li, *Chem. Soc. Rev.*, 2015, **44**, 633–6374.
8 Y. Da-Peng, C. Shouhui, H. Peng, W. Xiansong, J. Weiqiao, P. Omar and C. Daxiang, *Green Chem.*, 2010, **12**, 2038–2042.
9 F. Song, H. Su, J. Han, J. Xu and D. Zhang, *Sens. Actuators, B*, 2010, **145**, 39–45.
10 C. Yang, C. Choi, C. Lee and H. Yi, *ACS Nano*, 2013, **7**, 5032–5044.
11 C. Sun, H. Yang, Y. Yuan, X. Tian, L. Wang, Y. Guo, L. Xu, J. Lei, N. Gao, G. J. Anderson, X. Liang, C. Chen, Y. Zhao and G. Nie, *J. Am. Chem. Soc.*, 2011, **133**, 8617–8624.
12 X. Meng and D. Deng, *Chem. Mater.*, 2016, **28**, 3897–3904.
13 X. Zhang, X. He, Z. Kang, M. Cui, D. Yang and R. Luque, *ACS Sustainable Chem. Eng.*, 2019, **7**, 15762–15771.
14 G. Xue, Z. Yue, Z. Bing, T. Yiwei, L. Xiuying and L. Jianrong, *Analyst*, 2016, **141**, 1105–1111.
15 P. Intharapat, A. Kongnoo and K. Kateungngan, *J. Polym. Environ.*, 2013, **21**, 245–258.
16 D. Cree and A. Rutter, *ACS Sustainable Chem. Eng.*, 2015, **3**, 941–949.
17 L. Cao, Q. Ding, M. Liu, H. Lin and D. Yang, *ACS Appl. Bio Mater.*, 2021, **4**, 1424–1431.
18 X. He, D. Yang, X. Zhang, M. Liu, Z. Kang, C. Lin, N. Jia and R. Luque, *Chem. Eng. J.*, 2019, **369**, 621–633.
19 Y. Huang, Y. Ji, Z. Kang, F. Li, S. Ge, D. Yang, J. Ruan and X. Fan, *Chem. Eng. J.*, 2020, **395**, 125098.
20 Q. Ding, Z. Kang, L. Cao, M. Lin, H. Lin and D. Yang, *Appl. Surf. Sci.*, 2020, **510**, 145526.
21 Q. Ding, Z. Kang, X. He, M. Wang, M. Lin, H. Lin and D. P. Yang, *Mikrochim. Acta*, 2019, **186**, 453.
22 J. S. Markovski, D. D. Marković, V. R. Đokić, M. Mitrić, M. Ristić, A. E. Onjia and A. D. Marinković, *Chem. Eng. J.*, 2014, **237**, 430–442.
23 S. Zhong, J. Zhuang, D. Yang and D. Tang, *Biosens. Bioelectron.*, 2017, **96**, 26–32.
24 L. Cao, Z. Kang, Q. Ding, X. Zhang, H. Lin, M. Lin and D. Yang, *Sci. Total Environ.*, 2020, **723**, 138008.
25 P. Miao, K. Han, Y. Tang, B. Wang, T. Lin and W. Cheng, *Nanoscale*, 2015, **7**, 1586–1595.
26 J. Wu, M. Lin, X. Cong, H. Liu and P. Tan, *Chem. Soc. Rev.*, 2018, **47**, 1822–1873.
27 H. V. Le and Q. T. Le, *Adv. Polym. Technol.*, 2020, **2020**, 1–7.
28 L. Wang, M. Xu, Y. Xie, C. Qian, W. Ma, L. Wang and Y. Song, *Sens. Actuators, B*, 2019, **285**, 264–270.
29 A. Diouf, B. Bouchikhi and N. El Bari, *Mater. Sci. Eng., C*, 2019, **98**, 1196–1209.
30 H. Dai, P. Cao, D. Chen, Y. Li, N. Wang, H. Ma and M. Lin, *Synth. Met.*, 2018, **235**, 97–102.
31 W. Liu, G. Chai, X. Zhao, Y. Dai and Y. Qi, *Sens. Actuators, B*, 2020, **321**, 128485.
32 H. Chen, W. Su and Y. Yeh, *ACS Appl. Mater. Interfaces*, 2020, **12**, 32905–32914.
33 G. Pablo, R. Marcela, E. Marcos and R. Gustavo, *J. Pharm. Biomed. Anal.*, 2020, **191**, 113526.
34 A. Venkadesh, S. Radhakrishnan and J. Mathiyarasu, *Electrochim. Acta*, 2017, **246**, 544–552.
35 V. V. Khedekar and B. M. Bhanage, *J. Electrochem. Soc.*, 2016, **163**, B248–B251.
36 L. Tang, J. Lv, C. Kong, Z. Yang and J. Li, *New J. Chem.*, 2016, **40**, 6573–6576.